Addressing Thermal Distortion in Additive Manufacturing of Topology Optimized Structures Through Reverse Shape Morphing

Akhilesh Jha,[#] Gyanendra Pandey[#] and Harpreet Singh Bedi[$,*]

[#]*DRDO - Aeronautical Development Establishment (ADE), Bengaluru – 560 075, India*
[$]*Birla Institute of Technology and Science Pilani, Dubai Campus, Dubai, United Arab Emirates*
[*]*E-Mail: harpreet@dubai.bits-pilani.ac.in*

ABSTRACT

Design of light weight structures is an important aspect in the aircraft industry, since minimizing the weight of components improves the overall aircraft performance. However, conventional manufacturing methods work on standard geometries and shapes, and often lead to overdesigning of parts. Additive Manufacturing (AM) overcomes these issues by allowing more design freedom. The present study focuses on two aspects of AM: (1) part consolidation through topology optimization, and (2) addressing thermal distortion through reverse shape morphing. An assembly of two load bearing brackets is first amalgamated into a single Topology Optimized (TO) part, which satisfies the displacement and stress requirements of the original design. After a series of optimization iterations, the final TO part (278 g) weighs 69 % lesser than the original assembled design (909 g), still meeting the design constraints. The TO part thus eliminates the need of fasteners to join both the brackets, thereby, making the design simpler yet effective. Moreover, a homogeneous stress distribution in the optimized part allows for efficient material utilization. In order to overcome thermal distortion that results during the AM process, the shape of the TO part is transformed in a sense opposite to the distortions produced. This is achieved through reverse shape morphing technique, that reduces thermal distortions in the printed part to sub-micron levels, and the morphed TO part conforms to the requirements meeting the design constraints. Therefore, the implementation of topology optimization along with reverse shape morphing makes the design simple and efficient having reduced distortion. This is achieved without any need of modifications in the manufacturing system or equipment, and such a strategy can be replicated and implemented at industrial scale as well.

Keywords: Topology optimization; Additive manufacturing; Part consolidation; Powder bed fusion; Reverse shape morphing

1. INTRODUCTION

Modern day aerospace structures are subjected to complex static and dynamic loading patterns. The critical requirement of sustaining the allowable stresses and strains are to be met with very tight weight constraints. The requirement of lightweight designs, however, often leads to high level of geometrical complexity (with respect to structure, function, and property),[1,2] which makes it challenging to realize through conventional manufacturing methods. The parts fabricated through conventional methods, such as casting, rolling, forging, and machining, are limited to some standard geometries, sections and shapes.[3] The manufacturing process also has to take into consideration the manner in which different parts will be assembled and joined. This includes removable threaded fasteners, non-removable riveting, bonding using adhesives/brazing, and permanent joining through welding. However, such assemblies have lesser reliability and have higher inspection, tooling, and maintenance requirements.[4] Moreover, parts manufactured through such methods are subjected to inhomogeneous stress distribution, that may lead to dimensional

mismatch and deformations exceeding allowable tolerances[5]. Consequently, the use of continuous material to fabricate such a structure would lead to overdesigning,[6] leaving scope to make the part more efficient by selectively removing material from regions that are relatively less stressed.

This calls our attention towards the three basic types of structure optimization techniques: size optimization, shape optimization, and topology optimization[1]. Each of these optimization problems require the definition of an objective function (e.g. minimization of weight or stresses etc.) subjected to some constraints (e.g. threshold frequency, allowable deflection etc.). While a few dimensions of the part are optimized in size optimization, in shape optimization the shape of the bounding surfaces is varied to satisfy the objectives and constraints. On the other hand, topology optimization is a technique of distributing material optimally within a given design space satisfying the minimization or maximization objectives subject to certain constraints.[7] This allows a broader design space available with topology optimization compared to size and shape optimization techniques (which are limited to a sub-region of the full geometry), besides, topology optimization is independent of the original configuration itself. Topology optimization is mainly based on two approaches:

(1) truss-based method, (2) density-based method[1]. The truss-based approach generates a mesh of connected trusses in a given volume, and then iterates to find a set of trusses necessary for the problem while eliminating the others. During the process of truss optimization, the size of each truss member is varied, and as the optimization progresses smaller size trusses are removed. Patel *et. al.*[8] emphasized on varying both the truss size as well as its position during the optimization process. Alternatively, the density-based method fills a given volume with appropriate material density value. Such an approach works on the principle of solid isotropic material with penalization (SIMP) method in which the part geometry is divided into a set of voxels (a 3D version of a 2D pixel), with each voxel being assigned a density value between 0 (no material) and 1 (fully dense).[9] Optimization solutions with voxels that have density either 1 or close to 0 are desirable, so as to avoid partly dense materials that are often challenging to produce. Several studies have focused their attention on creating efficient topology optimization algorithms[10] for three dimensional problems[11] and problems involving multiple materials[12] as well.

Structurally optimized, but complex, shapes have organic or freeform designs that provide enhanced mechanical performance without compromising weight penalty[13]. Although topology optimized solutions can be manufactured through subtractive techniques, the implementation of topology optimization often leads to complex structural forms, which if manufactured additively allow the designer a considerable degree of freedom.[14] Owing to a variety of additive manufacturing (AM) processes available for polymer and metal printing such as binder jetting, material jetting, powder bed fusion, vat photopolymerization, etc.[15] AM is widely employed in the aerospace sector to serve the critical requirements of lightness and high specific strength/stiffness of the structural components, with aerospace industry contributing as much as 18 % to AM industry revenue.[16]

Laser powder bed fusion (PBF) is one method which can be used to produce complex shapes with reduced design and build time, on-demand manufacturing, instant assemblies, part consolidation, easy model changes and part customization, freedom of design, and increased buy-to-fly ratio with less material wastage.[17-18] PBF has been found to drastically reduce the material wastage to just 5 % compared to 95 % with conventional milling, with a buy-to-fly ratio close to 1:1.[19,20] However, the continuous cycle of melting and resolidification of powder layers causes anisotropic shrinkage,[21] thereby resulting in high temperature gradients[22] inducing residual stresses[23-25] and hence distortion[26] in the printed part. Apart from this some other factors that influence thermal distortion are: (1) material properties (heat capacity, thermal conductivity/diffusivity/expansion, elastic modulus), (2) processing parameters (part density, scan strategy, laser power, layer height, preheating, post-treatment), and (3) structure geometry (section length/thickness, part/support stiffness, laying angle)[27]. If not checked, the thermal distortions may result in tolerance errors[21], failure of support structure,[28] interlayer delamination, part-recoater interference,[27] voids and improper fusion[29-32].

Several techniques have been suggested to mitigate the effect of thermal distortion such as: laser scan strategy,[29,33-35] substrate preheating,[36-38] localized preheating of deposition region[39] etc. However, these methods are time consuming and are limited to small parts requiring modification in the laser deposition system. Further, the numerical modelling of additive manufacturing to find the ideal set of processing parameters[40-41] is limited to small part volumes, focuses on individual printed layers,[42-43] and are computationally expensive for full scale part modelling.[42,44] Data-driven statistical approach[45], and deep learning using big data[46] techniques have also been proposed, but need highly skilled manpower, high performance computing, and complex algorithms for distortion prediction and compensation. Dunbar *et al.*[47] demonstrated an experimental approach for distortion measurement, in which each scan pattern is rotated by 67°, though there is a need of specialised equipment. The authors also highlighted the importance of inter-layer effects to be included in thermo-mechanical models for better prediction of distortion[47]. Afazov, *et al.*[48] presented the idea of geometry compensation to minimize distortion, though the model is based on data inputs on materials, processing, and structural parameters. A simple technique lacks with which thermal distortions can be controlled without making any modifications in the manufacturing system or equipment, and can be readily implemented by the industry.

To this end, the present study illustrates the replacement of a sub-assembly of two brackets with a single TO component. The TO part, which is lighter and stiffer than the original design, is then virtually printed using laser powder bed fusion method by sequentially coupled thermo-mechanical simulations. Based on the thermal distortion analysis, reverse shape morphing technique is applied on the TO part to take care of the tolerance constraints and printing the part to meet the application requirements. Reverse shape morphing enables scaled deformation of a pre-existing shape without changing the topology. To the best of authors' knowledge, no literature is available on the use of reverse shape morphing as a tool to overcome thermal distortion in topology optimized additively manufactured parts. The findings of the present study can be implemented in any application involving structural load carrying members to attain simple yet efficient parts with least dimensional errors.

2. METHODOLOGY

The complete procedure followed for the preparation of additive manufacturing layout is shown in Fig. 1. Broadly, the methodology can be divided into 3 stages. In stage-1, the original model is set up by defining the boundary conditions, loading conditions and performing Finite Element Analysis (FEA) to get the part response in terms of displacement, stresses etc. This is followed by carrying out topology optimization procedure on a design space for a given set of targets to be achieved subject to constraints defined in the previous step.

The TO concept is analysed for any violation of design parameters. If the design criteria are not met, the above procedure is repeated either by modifying the targets or the design space itself. Once a feasible TO concept is attained satisfying the model functionality, the concept so generated is refined in stage-2 to get a topology optimized CAD model. The

refined part is again verified for any constraint violations.

In the final stage-3, the refined TO part is sent for virtual printing. The critical parameters to be considered here are part orientation, part slicing, generation of support structure, and laser scanning path. Once these parameters are defined, the part is virtually printed following the laser powder bed fusion technique by sequentially coupled thermo-mechanical simulations. Any excess thermal distortions are corrected by way of reverse shape morphing technique to get the optimum design. Each of these steps depicted in Fig. 1 is discussed in more detail in the coming sections.

3. ORIGINAL DESIGN

The sub-assembly taken for the case study consists of 2 brackets as shown in Fig. 2(a). Bracket-1 is bolted to the outer structural members of an airframe through 6 bolts, while bracket-2 consists of a bearing slot which acts as a hinge for the control surface sub-assembly of the aircraft wing. Bracket-2 is fixed rigidly to bracket-1 with 4 bolted connections shown in Fig. 2(c). Both the brackets are made of Aluminium alloy – Al 2014-T6. The bracket is designed as two separate parts so as to avoid excessive material removal during milling
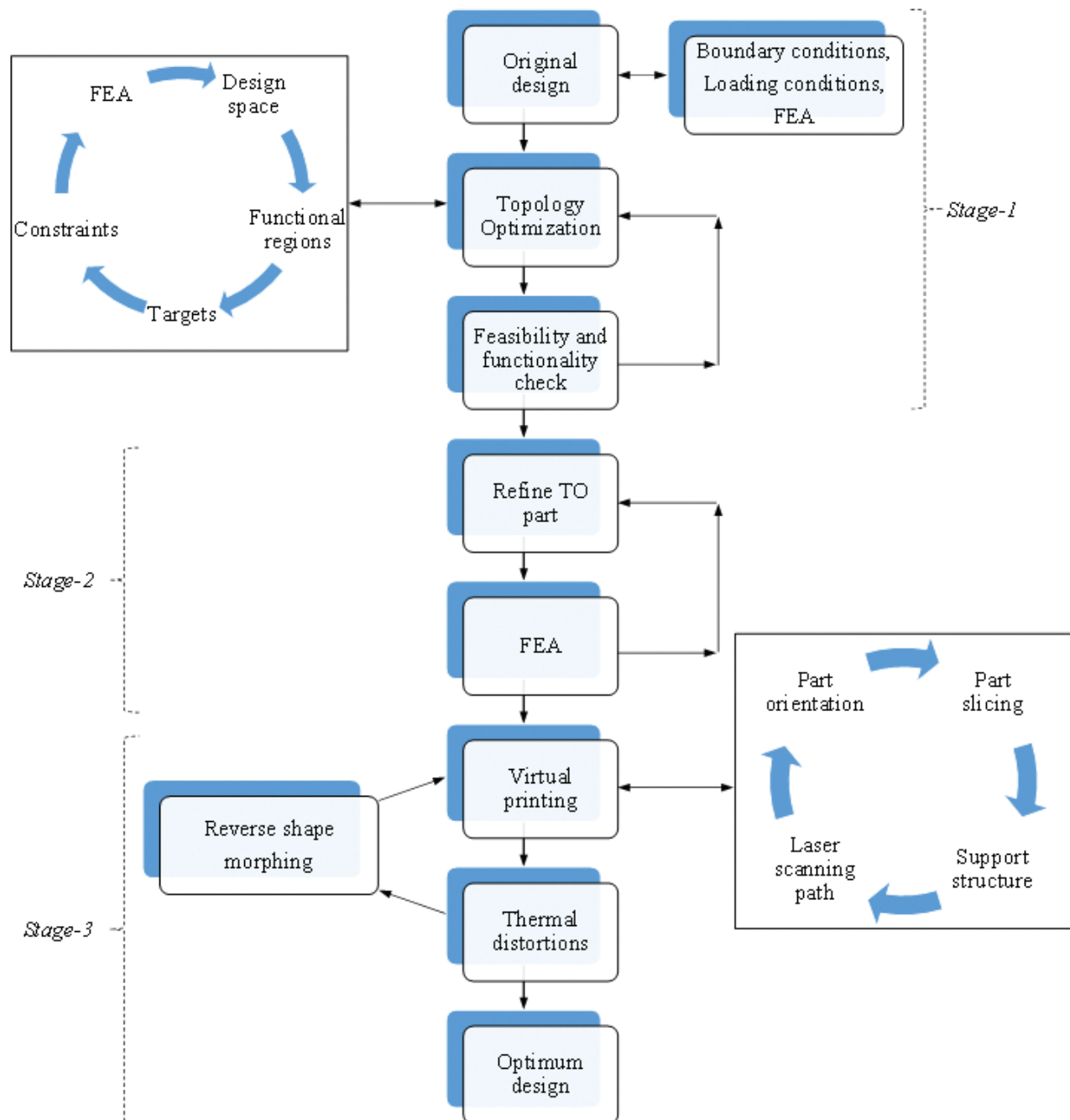

Figure 1. Methodology of additive manufacturing of a topology optimized part.

operation and keeping in mind the manufacturing constraints. Although, the present design is simple considering the CAD and manufacturability, this is a clear case of overdesigning having a total mass of 909 g.
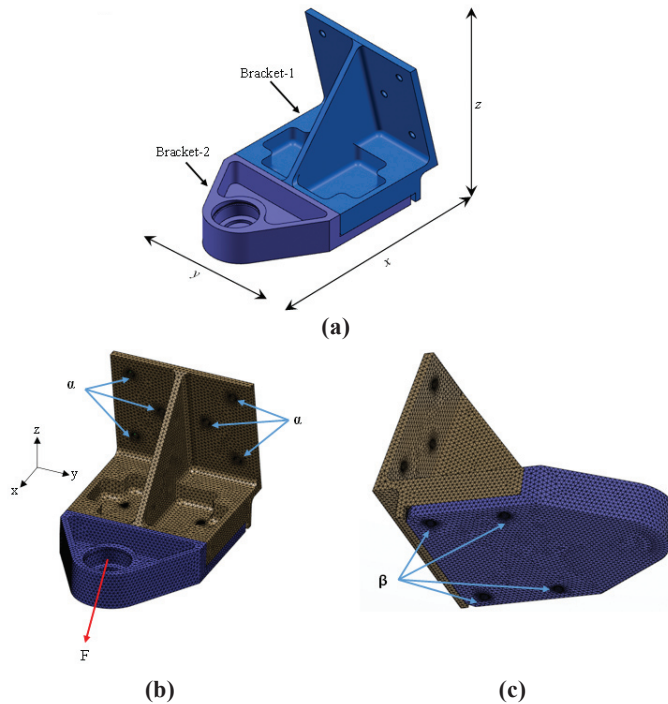

Figure 2. (a) CAD model of the original design of two brackets with dimensions x=180 mm, y=110 mm, z=120 mm, (b-c) Loading and boundary conditions applied on the meshed model of the original design: α – clamped boundary condition, β – bolted connections.

Static analysis is now performed on the original design to obtain the deformation and stress profiles which will later act as design constraints for the topology optimization problem. To this end, a finite element mesh is created with tetrahedron second order quadratic elements (TE10) for the original design as shown in Fig. 2(b-c). While, bracket-1 is clamped at 6 places, bracket-2 is bolted to bracket-1 through 4 infinitely stiff bolted connections. A force (F) acts on the hinge section of the bracket (Fig. 2b) having force components: F_x = -50 N, F_y = -2.52 N, F_z = -204 N. Figure 3 shows the displacement and
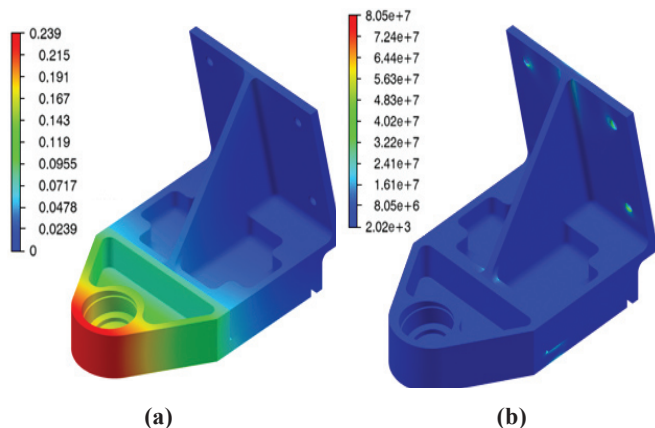

Figure 3. (a) Displacement and (b) stress distribution in the original design.

stress distribution in the original configuration. As expected, maximum displacement (~0.24 mm) is observed around the loading area, while maximum stress is 80 MPa and that too is concentrated at certain regions. This indicates the non-homogeneous stress distribution, and hence overdesigning. Therefore, there is a need to optimize the part in order to save weight and improve the performance of the part. In the next section, the topology optimization problem is defined in terms of objectives and constraints of the optimization problem, and design space and functional regions using the same loading and boundary conditions as given in Fig. 2.

4. TOPOLOGY OPTIMIZATION

The objective of the optimization problem at hand is to create a structurally stiff part with minimum weight under the given loading and boundary conditions. In other words, the optimized part must be able to withstand the deformation and stress levels as defined by the static analysis of the original configuration (refer Fig. 3). The solver[49] is, therefore, given a task of maximizing stiffness with a target mass of 35% of the design space. Symmetry constraint is used in the optimization process so that the generated conceptual part is symmetric about the mid-plane parallel to z-x plane in Fig. 4a.

4.1 Design Cycle-1

To begin with the optimization process, the first task is to conceptualize a design space, which captures the mechanical and functional requirements of the component. Design space is a volume or conceptual geometry in which the solver carries out the optimization by way of selective removal of material from non-critical areas. Here we propose a single solid design space that represents the original model such that it covers the area of both the brackets. This will help to consolidate the assembly of brackets into single structural member, which reduces the tool and part inventory as well as the associated costs[2,4], ultimately leading to increased reliability and performance[50]. Accordingly, a design space as shown in Fig. 4(a) is created and the material properties of aluminium alloy AlSi10Mg[51] are assigned (Table 1).

Table 1. Properties of AlSi10Mg additive manufacturing material

Property	ρ (kg/m³)	E (GPa)	ν	σ_y (MPa)	σ_t (MPa)
Value	2670	76	0.33	251	345

This is followed by assigning portions of the design space as functional region. Functional region is the region in the design space which is non-designable, that is, the solver is restricted from modifying this region during the optimization process as these regions serve the critical requirements. Accordingly, 7 functional regions are defined (see Fig. 4a): 6 bolt regions in bracket-1, and the bearing region in bracket-2. All these 7 regions are partitioned cylindrically with an offset of 3 mm and are assigned as functional regions. Additionally, the load bearing area is constrained because too much displacement in this region may affect the functionality of the part. The displacement along the hinge line is constrained to be less than the equivalent displacement in the original design.

Consequently, a set of nodes along the hinge line (highlighted in Fig. 4(b) is constrained for displacement not to exceed 0.2 mm.
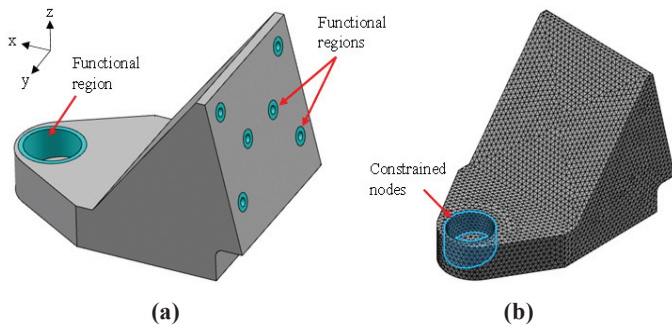

(a) **(b)**

Figure 4. (a) Design space and functional regions in the original configuration, and (b) Meshed model of the original design.

Once the design space, boundary and loading conditions, and performance targets are defined, the Tosca solver[49] performs a numerical methodology to remove any unwanted material from the design space that is not playing any useful function. Simple Isotropic Material with Penalization (SIMP) strategy is used by the solver to do topology optimization by varying the density between 0 (void space) and 1 (fully dense material) across the design space.[10] Figure 5 schematically shows the process flow during topology optimization followed on the design space given in Fig. 4. The fully dense material can be seen in red colour, while the material of no use is presented as blue in colour [Fig. 5(a)]. Over a number of iterations, the solver removes unwanted material and retains material only at regions necessary for the part to transmit the loads [Fig. 5(b-c)]. This indicates that no solid connection is needed between the upper and lower sets of bolts for transmitting the load.

The concept shape generated after the optimization process meeting all the objectives and constraints is shown in Fig. 5(d). The concept generated indicates that 4 bolt connections for bracket-1 are sufficient to efficiently provide stiffness under the applied loads. So, it is better to eliminate the middle two bolts [marked by arrows in Fig. 5(d)]. As per the conceptual shape, it will be difficult to fasten the bolts because of the presence of bulk material in front of lower holes [encircled regions in Fig. 5(d)] and slanting front face in front of top holes. Even though all the requirements are met, the concept is not practical to use. So, in order to get a workable design, the design space is modified as discussed in the next section.

4.2 Design Cycle-2

Based on the outcomes of design cycle-1, the design space is modified by eliminating the middle row of bolts and providing provision for bolt fastening. The updated design space, shown in Fig. 6a, is then subjected to topology optimization keeping the loading and boundary conditions, and objective and constraints as same from the previous design cycle-1. The concept shape so generated [Fig. 6(b)] not only meets targets and constraints, but is also viable both in terms of functional as well as the assembly requirements of the bracket. The maximum displacement of 0.037 mm [Fig. 6(c)] and maximum stress of ~24 MPa [Fig. 6(d)] are far lesser than

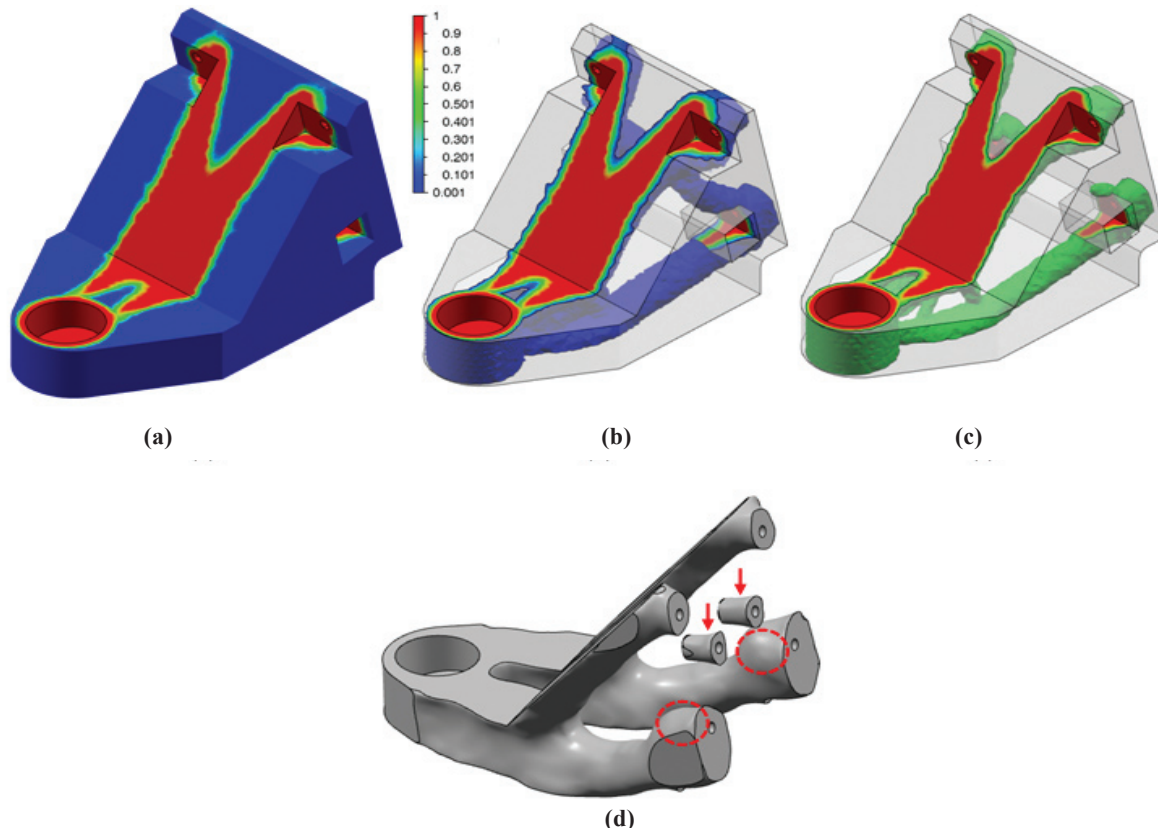

(a) **(b)** **(c)**

(d)

Figure 5. (a-c) Design cycle-1 process flow during topology optimization. Legend shows density level at different locations of the part during the optimization process, and (d) Concept generated after design cycle-1.

that produced in the original design (refer Fig. 3). However, these small magnitudes of displacement and stress, suggest underutilization of the material.

This motivates us to run another iteration of topology optimization with a reduced target of 25 % residual mass. The raw concept thereby generated after the second iteration is
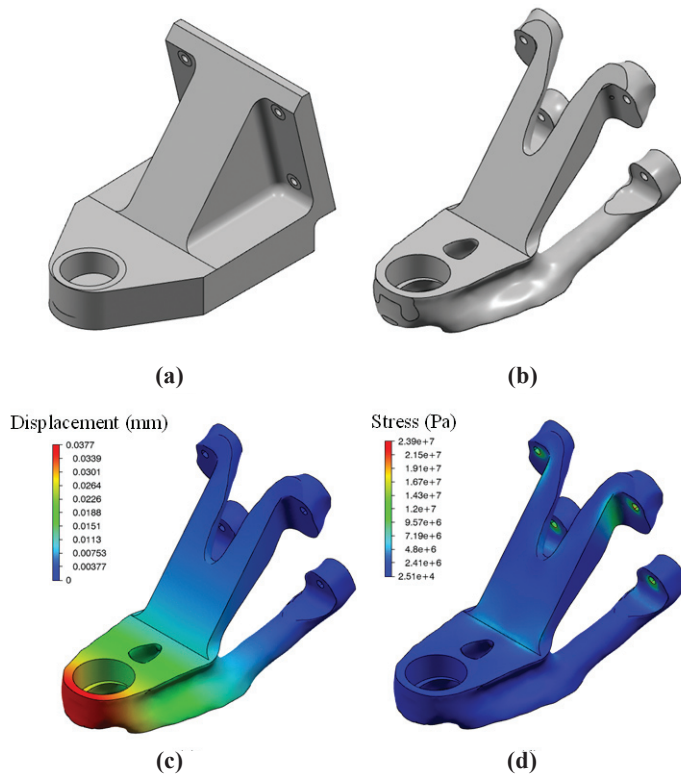

Displacement (mm)

Stress (Pa)

Figure 6. Design cycle-2, iteration-1: (a) Design space, (b) Topology optimized conceptual shape, and (c-d) Displacement and stress distribution in the generated concept.

shown in Fig. 7(a), which needs refinement by the designer to get a smooth CAD model as shown in Fig. 7b. Such refining process is carried out with the help of '*Imagine and Shape*'[49] toolbox so as to remove any unwanted tessellations or meshed surfaces.

Considering the conceptual shape as a guide part, the refined CAD part is prepared [Fig. 7(b)]. Static analysis is then performed on this refined model and the results are presented in Fig. 7. As expected, the displacement is high at the point of loading in the original design [0.239 mm, Fig. 3(a)] as well as in the topology optimized part [0.188 mm, Fig. 7(c)]. This 21 % reduction in peak displacement indicates an improved stiffness of the TO part with respect to the original configuration. Even though the peak displacement [Fig. 7(c)] and peak stress (Fig. 7d) obtained in *design cycle-2* are more than the previous iteration, these are still less than the requirements of the original design. Furthermore, the stress gets transferred away from the loaded region to the arms of the part and is homogenously distributed throughout the part [Fig. 7(d)]. The refined TO part weighs 278 g, which means a 69% reduction in mass compared to the original design (Fig. 2). Figure 7(e) shows the conformance between the TO part and the original design in terms of bolted and load application regions. Figure

7(e) also highlights the simplicity of the TO part in contrast to the original design configuration of the sub-assembly of brackets.
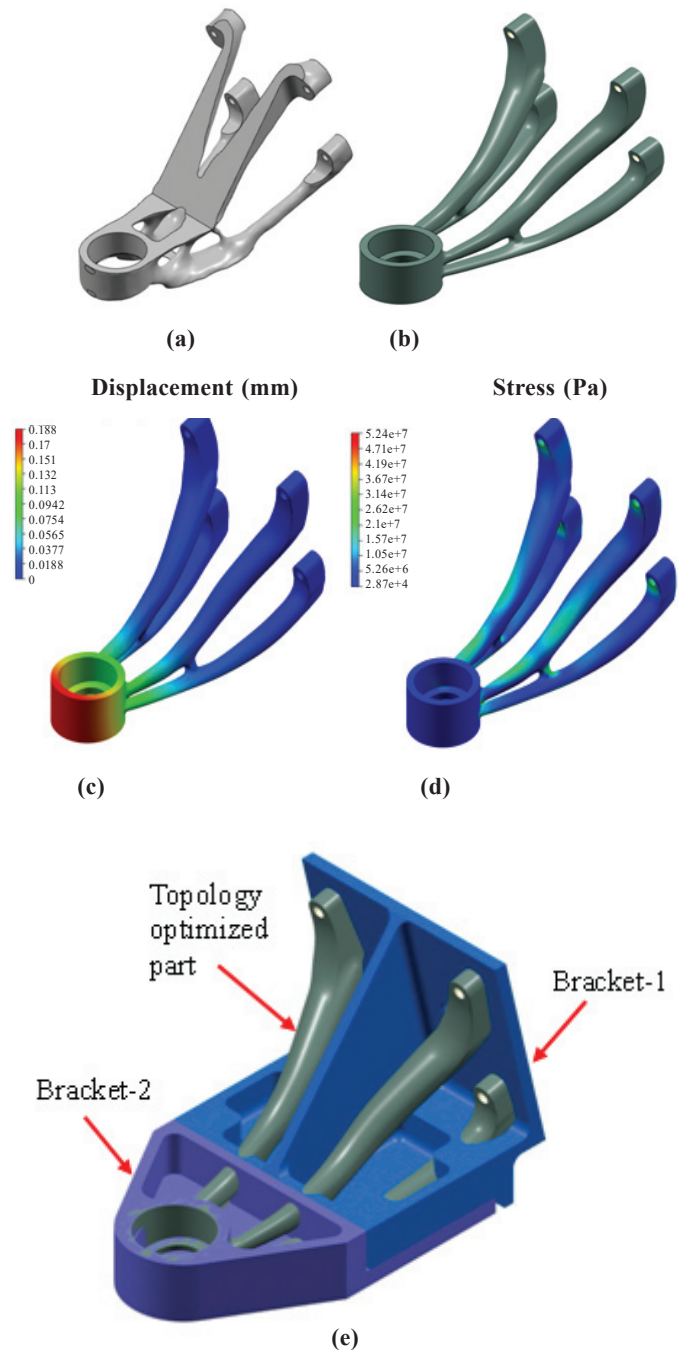

Displacement (mm)

Stress (Pa)

Figure 7. Design cycle-2, iteration-2: (a) Topology optimized conceptual shape, (b) Refined topology optimized concept, (c-d) Displacement and stress distribution in the refined concept, and (e) Topology optimized part superimposed on the original design of the pair of brackets.

5. VIRTUAL PRINTING
5.1 Part Orientation

Part orientation is one of the most critical parameters in additive manufacturing. Ideally, the best orientation is the one leading to minimum effective height of the printed part, thereby resulting in minimum printing time and hence cost.

This, however, must not be the sole factor to decide the part orientation as it directly affects not only the surface quality and the volume of supports required, but the mechanical properties of the printed part as well.[3,18] Table 2 shows various parameters and their priority level considered to define part orientation.[52] Since, the part dimensions can be easily accommodated in the machine (SLM280: 280 mm x 280 mm x 365 mm), and there are no sudden cross-section changes in the part, low priority is assigned to three parameters: projected part area, part height, and slice variation. Member to member support criteria is assigned medium priority because the gap between different members of the part varies from one end (loaded region) to the other end (fixed end), and no hollow regions to be supported other than the loaded region. Finally, to minimize the supports required for the part, highest priority is given to part area requiring support. Keeping in mind these considerations, the solver[52] suggests the orientation of part on build tray as shown in Fig. 8.

Table 2. **Selection criteria for the computation of part orientation for virtual printing**

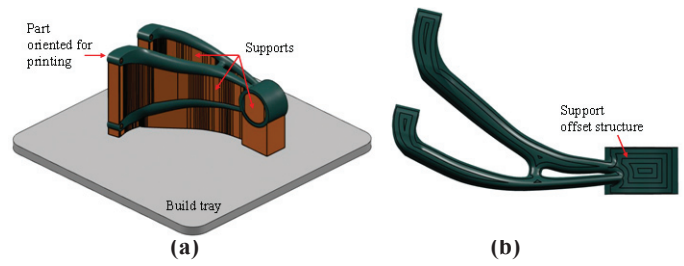| Criteria	Priority level
Part area requiring support	High
Part area projected on build tray	Low
Member to member support area within a part	Medium
Part height	Low
Slice variation	Low

Figure 8. (a) Part orientation and support structure used for printing the refined topology optimized concept on build tray, and (b) Offset patterned structure of the supports shown on the bottom view of the part.

5.2 Support Structure

To carry out the additive manufacturing of the part, a support structure is required to support the part on the build tray, support the part overhangs and to carry the heat away from the part.[6] For the given part orientation, a support structure is generated [Fig. 8(a)] using wired-offset[52] patterned support structure [Fig. 8(b)] with a spacing of 3 mm between the successive support walls. Such patterns, having line contact between the support and the part, provide higher strength than point contact supports and are easy to remove when compared to area contact supports.[53]

5.3 Laser Scanning Path

After finalizing the part orientation and support structure, the laser scanning path is generated. A 400 W, 0.09 mm diameter laser beam is used to scan the powder bed at a scan speed of 10 m/s.[52] A typical scan strategy includes contours and infill (see Fig. 9). Figure 9 shows the scan path at different levels of
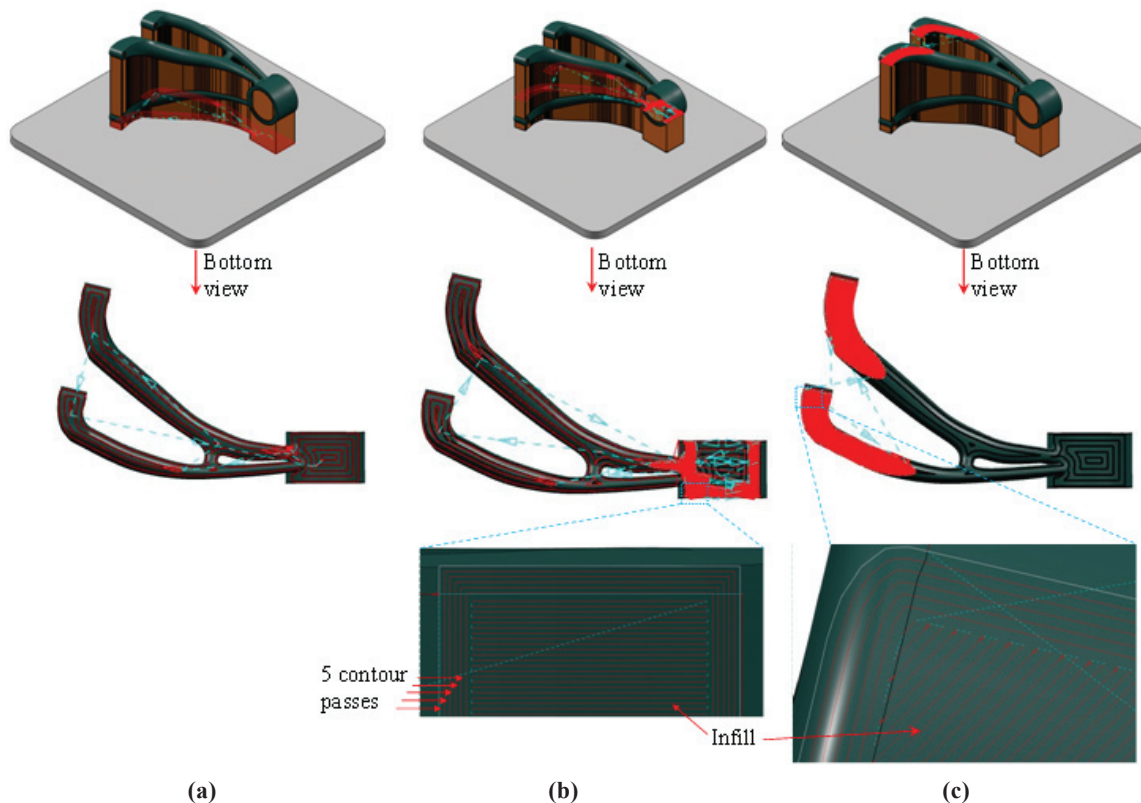

Figure 9. Laser scanning path for the part and supports to be printed at different part heights: (a) At the interface of support structure and the build-tray, (b) In the middle of the part, and (c) Near the top region of the part.

part height: (a) at the interface of support structure and the build-tray, (b) in the middle of the part, and (c) near the top region of the part. As can be seen in the detailed views of Fig. 9 (b-c), 5 contour passes are used to print the outer boundary. While, contours are meant to make an outer boundary and give smooth surfaces to the part, the core of the part is filled with a hatching pattern.

5.4 Virtual printing

A finite element mesh of the part is now generated with tetrahedron (TE4) elements having 4 nodes (see Fig. 10a). While, the supports are meshed using quad dominant elements having a mix of trigonal (TR3) and quad (QD4) elements, the build tray is meshed using sweep 3D elements with a mix of wedge (WE6) and hexahedral (HE8) elements.[52] Next, the bottom face of the build tray is clamped, and tie constraints are generated between the tray and supports, and between supports and the part. The tie constraints replicate the actual printing conditions of fusion between the tray and supports, and between supports and the part. The following printing parameters are given as input[52]: powder melting temperature = 1200°K, powder absorption coefficient = 0.45, convection coefficient of inert (argon) gas = 18 W/°K/m^2, powder emissivity = 0.25. The thermal and mechanical steps are then defined to perform the thermo-mechanical analysis. An initial time increment of 200 s is used for a total simulation time of 4428 s.

After defining all these input parameters, the printing procedure begins based on powder bed fusion technique. In this technique, a layer of metallic powder is spread uniformly on the build tray and a laser is used to melt the powder particles. As the laser travels across a predetermined scan path, molten melt fuses and solidifies to make a slice or layer of the part. Once a layer is formed, the tray is moved downward equal to the slice thickness, powder is spread again and the laser

scanning and melting process is repeated till the whole part is manufactured. Figure 10b-c shows the printed supports and the part along with temperature [Fig. 10(b)] and displacement [Fig. 10(c)] distributions on the part. As can be seen in Fig. 10b the temperature in the lower portion of the part is lowest and is similar to that of build tray. Whereas, near the top portion of the part the temperature is relatively high, as these are the most recent printed layers. This temperature variation in the printed part leads to thermal distortions with higher distortion in the right-side portion of the printed part [see Fig. 10(c)]. With a maximum distortion value of ~0.95 mm and an average distortion of ~0.5 mm, the right-side portion of the part does not conform to the desired shape of the topology optimized part shown in Fig. 7b. This may result in tolerance errors, failure of support structure,[28] interlayer delamination, part-recoater interference, voids, and improper fusion.[29-31] Similar bending of far ends of the printed part is observed both in experimental studies[54] as well as through prediction analysis.[55] In order to mitigate the effect of thermal distortion, reverse shape morphing is used to compensate for the predicted part distortions.

6. REVERSE SHAPE MORPHING

In the process of compensating the part distortions, the displacement field of the printed topology optimized (TO) part (Fig. 10c) is extracted. The displacement field consists of position coordinates of all the nodes present in the model. A scale factor is then applied on the displacement field to change the nodal displacements[56]. A negative scale factor = -1 results in computing the displacements in the opposite direction. Figure 11 compares the shape difference between the TO part (Fig. 7b), printed TO part (Fig. 10c), morphed part (Fig. 11c), and printed morphed part (Fig. 11d). The distortions in the right-side portion of the printed TO part with respect to
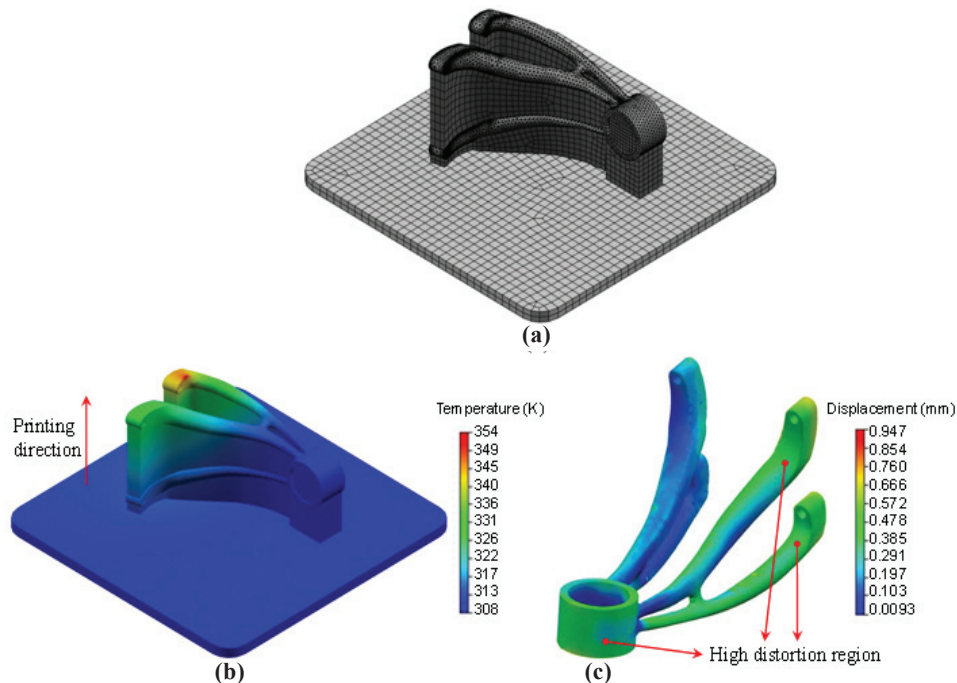

Figure 10. (a) Meshed model of the topology optimized part, support structure and build tray. Distribution of: (b) Temperature, and (c) Displacement in the printed topology optimized part.

the TO part, as pointed out in the previous section (see Fig. 10c), are clearly depicted in Fig. 11a where both the concepts are superimposed. Figure 11b shows the deviation analysis between the compensated geometry (printed TO part) and the original geometry (TO part). A lot of deviation can be seen in the circular load carrying region (+0.4 mm, yellow region) and right portion (-0.4 mm, cyan region) of the part.
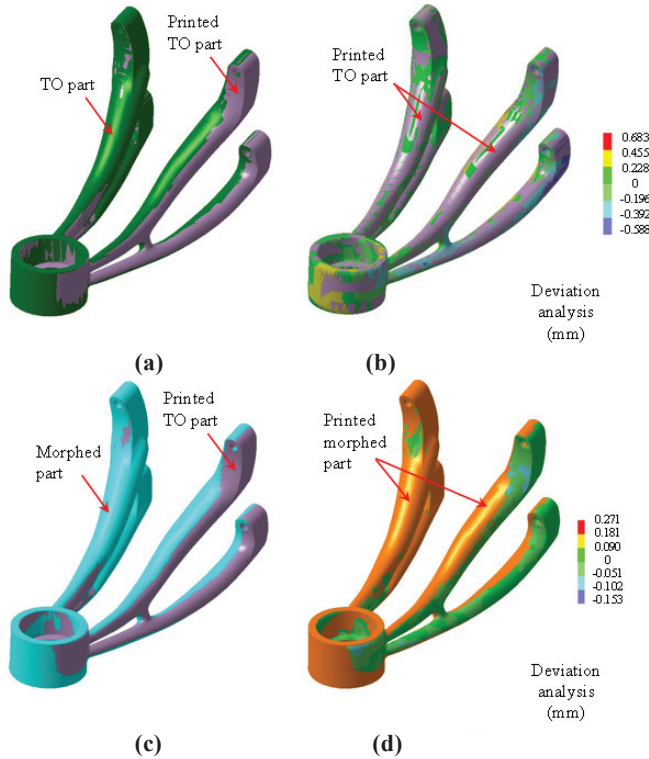

Figure 11. Shape distortion of: (a) Topology optimized (TO) part (green colour) and (c) Morphed part (cyan colour) with respect to printed TO part (purple colour). Deviation analysis of: (b) Printed TO part (purple colour) and (d) Printed morphed part (orange colour) with respect to the TO part.

This requires the original geometry to be negatively morphed before being printed, so that the printed part conforms the shape of the original geometry i.e. TO part shown in Fig. 7b. As expected, the morphed part appears distorted toward left side from the printed TO part (Fig. 11c). The morphed part is then printed as per details given in section-5.4. The deviation analysis between the printed morphed part (compensated geometry) and the TO part (original geometry) shows close proximity between the two (Fig. 11d). This is further validated in terms of displacements in the printed morphed part given in Fig. 12b. The peak displacement in printed morphed part (0.0578 mm) has drastically reduced by ~16 times, compared to 0.947 mm in printed TO part (Fig. 10c). Moreover, the displacement range of printed morphed part has narrowed down to 13 – 57.8 µm, contrary to large displacement variations of 0.103 – 0.947 mm in the printed TO part. The point to be noted here is that, shape morphing not only reduces the displacement magnitude, but also narrows down the range of displacements to which the single part is subjected over its length from the point of fixation to the point of loading.
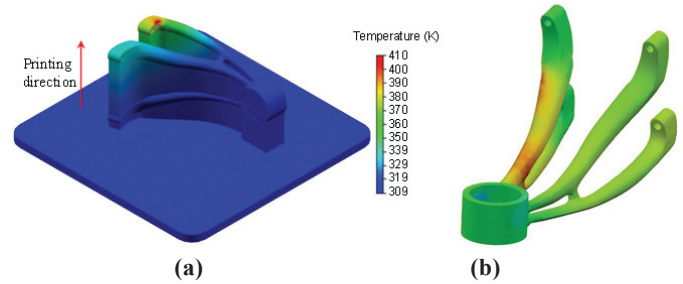

Figure 12. Distribution of: (a) Temperature, and (b) Displacement in the printed morphed part.

7. CONCLUSION

Topology optimization is used to redesign a sub-assembly of load carrying brackets. The original pair of brackets is modified so as to get a single consolidated topology optimized (TO) part requiring lesser number of fasteners. The design space and the optimization targets are varied so as to accommodate the functionality and practicality in the TO concept. The final TO part weighs only 278 g, which is 69 % lighter than the original design (909 g), yet meeting the design constraints. A maximum displacement of 0.19 mm near the point of applied load is within the upper limit of 0.24 mm in the original design. Also, the maximum stress in the TO part (52 MPa) is 35 % less compared to the original design (80 MPa). Moreover, a homogeneous stress distribution throughout the optimized part allows for efficient material utilization. The TO part is then virtually printed through powder bed fusion technique. A suitable part orientation and support structure is chosen by assigning different priority levels to key selection parameters. Reverse shape morphing technique is used to compensate the geometry of the TO part for the predicted thermal distortions. This is done by scaling the dimensions of the TO part by negative one, before being printed. The approach helps in bringing down the thermal distortions in the additively manufactured part to sub-micron levels. Hence, by integrating topology optimization with reverse shape morphing, simple, light weight and efficient designs can be additively manufactured to serve the critical requirements of the aircraft industry.

REFERENCES

1. Gibson, I.; Rosen, D. & Stucker, B. Additive manufacturing technologies: 3d printing, rapid prototyping, and direct digital manufacturing. Springer, 2015. doi:https://doi.org/10.1007/978-1-4939-2113-3

2. Liu, R.; Wang, Z.; Sparks, T.; Liou, F. & Newkirk, J. Aerospace applications of laser additive manufacturing. *In* Brandt, M. (ed) Laser Additive Manufacturing. Woodhead Publishing, 2017, pp.351-71.

doi: 10.1016/B978-0-08-100433-3.00013-0

3. Badiru, A.B.; Valencia, V.V. & Liu, D. Additive manufacturing handbook: product development for the defense industry. CRC Press, 2017.

4. Shapiro, A.A.; Borgonia, J.; Chen, Q.; Dillon, R.; Mc Enerney, B.; Polit-Casillas, R. & Soloway, L. Additive manufacturing for aerospace flight applications. *J. Spacecr. Rockets*, 2016, 952-59.
    doi: 10.2514/1.A33544

5. Saadat, M. Challenges in the assembly of large aerospace components. Integrated systems, design and technology 2010. Springer, 2011, pp.37-46. doi:https://doi.org/10.1007/978-3-642-17384-4_4

6. Yang, L.; Hsu, K.; Baughman, B.; Godfrey, D.; Medina, F.; Menon, M. & Wiener, S. Additive manufacturing of metals: the technology, materials, design and production. Springer, 2017.

7. Pelleg, J. Additive and traditionally manufactured components: A comparative analysis of mechanical properties. Additive manufacturing materia, 2020.

8. Patel, J. & Choi, S.-K. Classification approach for reliability-based topology optimization using probabilistic neural networks. *Struct. Multidiscipl. Optim.*, 2012, **45**(4), 529-43.
    doi: 10.1007/s00158-011-0711-2

9. Zegard, T. & Paulino, G.H. Bridging topology optimization and additive manufacturing. *Struct. Multidiscipl. Optim.*, 2016, **53**(1), 175-92.
    doi: 10.1007/s00158-015-1274-4

10. Sigmund, O. A 99 line topology optimization code written in Matlab. *Struct. Multidiscipl. Optim.*, 2001, **21**(2), 120-27.
    doi: 10.1007/s001580050176

11. Liu, K. & Tovar, A. An efficient 3D topology optimization code written in Matlab. *Struct. Multidiscipl. Optim.*, 2014, **50**(6), 1175-96.
    doi: 10.1007/s00158-014-1107-x

12. Raeisi, S., Tapkir, P., Tovar, A., Mozumder, C. & Xu, S. Multi-Material Topology Optimization for Crashworthiness Using Hybrid Cellular Automata. Report no. 0148-7191, 2019. SAE Technical Paper.
    doi: 10.4271/2019-01-0826

13. Adam, G.A.O. & Zimmer, D. Design for additive manufacturing—element transitions and aggregated structures. *CIRP J. Manuf. Sci. Technol.*, 2014, **7**(1), 20-28.
    doi: 10.1016/j.cirpj.2013.10.001

14. Wu, T.; Liu, K. & Tovar, A. Multiphase topology optimization of lattice injection molds. *Comput. Struct.*, 2017, **192**, 71-82.
    doi: 10.1016/j.compstruc.2017.07.007

15. Standard terminology for additive manufacturing technologies, ASTM F2792-12. American Society of Testing and Materials, 2012. https://www.astm.org/f2792-12.html

16. Najmon, J.C., Raeisi, S. & Tovar, A. Review of additive manufacturing technologies and applications in the aerospace industry. *In* Froes, F. & Boyer, R. (eds) Additive Manufacturing for the Aerospace Industry. Elsevier, 2019, pp.7-31.
    doi: 10.1016/B978-0-12-814062-8.00002-9

17. Hanush, S.S. & Manjaiah, M. Topology optimization of aerospace part to enhance the performance by additive manufacturing process. *Mater. Today: Proc.*, 2022,
    doi: 10.1016/j.matpr.2022.02.074

18. Diegel, O.; Nordin, A. & Motte, D. A practical guide to design for additive manufacturing. Springer, 2019.
    doi: 10.1007/978-981-13-8281-9

19. Jan, H.; Jouni, P.; Jukka, T. & Manfred, W. Rapid manufacturing in the spare parts supply chain: Alternative approaches to capacity deployment. *J. Manuf. Technol. Manag.*, 2010, **21**, 687-97.
    doi: 10.1108/17410381011063996

20. Nickels, L. AM and aerospace: an ideal combination. *Met. Powder Rep.*, 2015, **70**(6), 300-03.
    doi: 10.1016/j.mprp.2015.06.005

21. Paul, R.; Anand, S. & Gerner, F. Effect of thermal deformation on part errors in metal powder based additive manufacturing processes. *J. Manuf. Sci. Eng.*, 2014, **136**(3).
    doi: 10.1115/1.4026524

22. Khan, H.M.; Waqar, S. & Koç, E. Evolution of temperature and residual stress behavior in selective laser melting of 316L stainless steel across a cooling channel. *Rapid Prototyp. J.*, 2022.
    doi: 10.1108/RPJ-09-2021-0237

23. Denlinger, E.R.; Heigel, J.C. & Michaleris, P. Residual stress and distortion modeling of electron beam direct manufacturing Ti-6Al-4V. *Proc. Inst. Mech. Eng., Part B*, 2015, **229**(10), 1803-13.
    doi: 10.1177/0954405414539494

24. Shiomi, M.; Osakada, K.; Nakamura, K.; Yamashita, T. & Abe, F. Residual stress within metallic model made by selective laser melting process. *CIRP Ann.*, 2004, **53**(1), 195-98.
    doi: 10.1016/S0007-8506(07)60677-5

25. Zou, S.; Xiao, X.; Li, Z.; Liu, M.; Zhu, C.; Zhu, Z.; Chen, C. & Zhu, F. Comprehensive investigation of residual stress in selective laser melting based on cohesive zone model. *Mater. Today Commun.*, 2022, **31**, 103283.
    doi: 10.1016/j.mtcomm.2022.103283

26. Denlinger, E.R. & Michaleris, P. Mitigation of distortion in large additive manufacturing parts. *Proc. Inst. Mech. Eng., Part B*, 2017, **231**(6), 983-93.
    doi: 10.1177/0954405415578580

27. Xie, D.; Lv, F.; Yang, Y.; Shen, L.; Tian, Z.; Shuai, C.; Chen, B. & Zhao, J. A review on distortion and residual stress in additive manufacturing. *Chin. J. Mech. Eng.*, 2022, 100039.
    doi: 10.1016/j.cjmeam.2022.100039

28. Calignano, F. Design optimization of supports for overhanging structures in aluminum and titanium alloys by selective laser melting. *Mater. Des.*, 2014, **64**, 203-13.
    doi: 10.1016/j.matdes.2014.07.043

29. Kruth, J.-P.; Froyen, L.; Van Vaerenbergh, J.; Mercelis, P.; Rombouts, M. & Lauwers, B. Selective laser melting

of iron-based powder. *J. Mater. Process. Technol.*, 2004, **149**(1-3), 616-22.
doi: 10.1016/j.jmatprotec.2003.11.051

30. Yadroitsev, I.; Bertrand, P. & Smurov, I. Parametric analysis of the selective laser melting process. *Appl. Surf. Sci.*, 2007, **253**(19), 8064-69.
doi: 10.1016/j.apsusc.2007.02.088

31. Deo, M. & Michaleris, P. Mitigation of welding induced buckling distortion using transient thermal tensioning. *Sci. Technol. Weld. Joining*, 2003, **8**(1), 49-54.
doi: 10.1179/136217103225008919

32. Dunbar, A.J. Study of the evolution of distortion during the powder bed fusion build process using a combined experimental and modeling approach. Thermo-mechanical modeling of additive manufacturing. Elsevier, 2018, pp.229-50.
doi: 10.1016/B978-0-12-811820-7.00017-3

33. Nickel, A.; Barnett, D. & Prinz, F. Thermal stresses and deposition patterns in layered manufacturing. *Mater. Sci. Eng. A*, 2001, **317**(1-2), 59-64.
doi: 10.1016/S0921-5093(01)01179-0

34. Dai, K. & Shaw, L. Distortion minimization of laser-processed components through control of laser scanning patterns. *Rapid Prototyp. J.*, 2002,
doi: 10.1108/13552540210451732

35. Foroozmehr, E. & Kovacevic, R. Effect of path planning on the laser powder deposition process: thermal and structural evaluation. *Int. J. Adv. Manuf. Technol.*, 2010, **51**(5-8), 659-69.
doi: 10.1007/s00170-010-2659-6

36. Vasinonta, A.; Beuth, J.L. & Griffith, M. Process maps for predicting residual stress and melt pool size in the laser-based fabrication of thin-walled structures. *J. Manuf. Sci. Eng.*, 2007,
doi: 10.1115/1.2335852

37. Jendrzejewski, R.; Śliwiński, G.; Krawczuk, M. & Ostachowicz, W. Temperature and stress fields induced during laser cladding. *Comput. Struct.*, 2004, **82**(7-8), 653-58.
doi: 10.1016/j.compstruc.2003.11.005

38. Jendrzejewski, R. & Śliwiński, G. Investigation of temperature and stress fields in laser cladded coatings. *Appl. Surf. Sci.*, 2007, **254**(4), 921-25.
doi: 10.1016/j.apsusc.2007.08.014

39. Aggarangsi, P. & Beuth, J.L. Localized preheating approaches for reducing residual stress in additive manufacturing. *In* 2006 International Solid Freeform Fabrication Symposium 2006.
doi: 10.26153/tsw/7174

40. Zhang, D., Cai, Q., Liu, J., Zhang, L. & Li, R. Select laser melting of W–Ni–Fe powders: simulation and experimental study. *Int. J. Adv. Manuf. Technol.*, 2010, **51**(5-8), 649-58.
doi: 10.1007/s00170-010-2641-3

41. Dai, D. & Gu, D. Thermal behavior and densification mechanism during selective laser melting of copper matrix composites: simulation and experiments. *Mater. Des.*, 2014, **55**, 482-91.

doi: 10.1016/j.matdes.2013.10.006

42. Roberts, I.A.; Wang, C.; Esterlein, R.; Stanford, M. & Mynors, D. A three-dimensional finite element analysis of the temperature field during laser melting of metal powders in additive layer manufacturing. *Int. J. Mach. Tools Manuf.*, 2009, **49**(12-13), 916-23.
doi: 10.1016/j.ijmachtools.2009.07.004

43. Li, C.; Fu, C.; Guo, Y. & Fang, F. A multiscale modeling approach for fast prediction of part distortion in selective laser melting. *J. Mater. Process. Technol.*, 2016, **229**, 703-12.
doi: 10.1016/j.jmatprotec.2015.10.022

44. Denlinger, E.R.; Irwin, J. & Michaleris, P. Thermomechanical modeling of additive manufacturing large parts. *J. Manuf. Sci. Eng.*, 2014, **136**(6),
doi: 10.1115/1.4028669

45. Wang, C.; Li, S.; Zeng, D. & Zhu, X. Quantification and compensation of thermal distortion in additive manufacturing: A computational statistics approach. *Comput. Methods Appl. Mech. Eng.*, 2021, **375**, 113611.
doi: 10.1016/j.cma.2020.113611

46. Francis, J. & Bian, L. Deep learning for distortion prediction in laser-based additive manufacturing using big data. *Manuf. Lett.*, 2019, **20**, 10-14.
doi: 10.1016/j.mfglet.2019.02.001

47. Dunbar, A.J.; Denlinger, E.R.; Heigel, J.; Michaleris, P.; Guerrier, P.; Martukanitz, R. & Simpson, T.W. Development of experimental method for in situ distortion and temperature measurements during the laser powder bed fusion additive manufacturing process. *Addit. Manuf.*, 2016, **12**, 25-30.
doi: 10.1016/j.addma.2016.04.007

48. Afazov, S.; Denmark, W.A.D.; Lazaro Toralles, B.; Holloway, A. & Yaghi, A. Distortion prediction and compensation in selective laser melting. *Addit. Manuf.*, 2017, **17**, 15-22.
doi: 10.1016/j.addma.2017.07.005

49. Function Driven Generative Designer, 3DEXPERIENCE platform, dassault systemes, https://my.3dexperience.3ds.com/welcome/compass-world/rootroles/function-driven-generative-designer?role=true

50. Duda, T. & Raghavan, L.V. 3D metal printing technology. *IFAC-PapersOnLine*, 2016, **49**(29), 103-10.
doi: 10.1016/j.ifacol.2016.11.111

51. Additive manufacturing analysis engineer, 3Dexperience platform, dassault systems, https://my.3dexperience.3ds.com/welcome/compass-world/rootroles/additive-manufacturing-analysis-engineer?role=true

52. Powder bed machine specialist, 3DEXPERINCE platform, dassault systemes, https://my.3dexperience.3ds.com/welcome/compass-world/3dexperience-industries/aerospace-and-defense/ready-for-rate/additive-manufacturing/powder-bed-machine-specialist

53. Krol, T.; Zaeh, M. & Seidel, C. Optimization of supports in metal-based additive manufacturing by means of finite element models. *In* 2012 International Solid Freeform Fabrication Symposium University of Texas at Austin, 2012. doi:http://dx.doi.org/10.26153/tsw/15383

54. Wu, A.S.; Brown, D.W.; Kumar, M.; Gallegos, G.F. & King, W.E. An experimental investigation into additive manufacturing-induced residual stresses in 316L Stainless Steel. *Metall. Mater. Trans. A*, 2014, **45**(13), 6260-70. doi: 10.1007/s11661-014-2549-x

55. Montevecchi, F.; Venturini, G.; Grossi, N.; Scippa, A. & Campatelli, G. Finite element mesh coarsening for effective distortion prediction in wire arc additive manufacturing. *Addit. Manuf.*, 2017, **18**, 145-55. doi: 10.1016/j.addma.2017.10.010

56. Digitized morphing, CATIA-V5, dassault systemes, http://catiadoc.free.fr/online/rsoug_C2/rsougrf0100.htm

CONTRIBUTORS

Mr Akhilesh Kumar Jha is presently working as a senior scientist at Aeronautical Development Establishment, Bengaluru, India in the field of UAV design and development. He has done BTech from NIT Jamshedpur in mechanical engineering and MTech from IIT Mumbai in aerospace structures. He has extensive experience in the design and development of airframes, control surfaces, landing gear, fuel tank, and digital mock-up generation for MALE-UAV. He has also worked as system engineer for imported and indigenous payloads. He has published more than 20 papers in different national and international conferences, seminars and journals. He has also been awarded lab scientist award for the year 2016. He is a member of Aeronautical Society of India as well as Indian Society for Advancement of Materials and Processes.
For the current study, he was involved in supervision, project administration, and funding acquisition

Mr Gyanendra Pandey is presently working as a Scientist at Aeronautical Development Establishment, Bengaluru, India in the field UAV design and development. He has done B.Tech from KNIT Sultanpur in mechanical engineering and M Tech from IIT Kanpur in Solid Mechanics & Design. He has a vast experience in the design and development of airframes structure, engine mounting frame & various other subsystems for UAV and Missile systems. He has been awarded lab scientist award for the year 2015. He is an active member of Aeronautical Society of India.
For the current study, he supervised and did analysis.

Dr Harpreet Singh Bedi is an Assistant Professor in the Department of Mechanical Engineering at BITS Pilani Dubai campus, United Arab Emirates. Prior to this, he worked as Research Associate for two years at Aeronautical Development Establishment, DRDO, India. He completed his PhD (2020) from Indian Institute of Technology Ropar specializing in fabrication, testing and characterization of reinforced polymer composites. His research interests include nanofiller and fiber reinforced plastics, advanced composites, topology optimization and additive manufacturing. He has published more than 30 research articles in various international journals and conferences.
For the current study, he was involved in conceptualization of problem, development of methodology, simulations, analysis, manuscript draft, and manuscript reviews.